

Microscopic fracture studies in the two-dimensional triangular lattice*

William T. Ashurst

Sandia Livermore Laboratory, Livermore, California 94550

William G. Hoover

Department of Applied Science, University of California at Davis/Livermore,
and Lawrence Livermore Laboratory, Livermore, California 94550

(Received 22 March 1976)

In order to understand the static and dynamic bases of macroscopic fracture mechanics, we study flawed microscopic crystals obeying Newton's equations of motion. The particles in these crystals interact with truncated Hooke's-law forces. The static results for energy, entropy, stress concentration, and crack structure are all consistent with expectations from macroscopic elasticity theory. Dynamic theory is less well developed. Our dynamic results illustrate the importance of surface energy and nonlinear terms in the interparticle forces in influencing crack morphology and propagation velocity. The propagating cracks, except in crystals preloaded nearly to the theoretical tensile strength, travel at speeds somewhat less than the long-wavelength Rayleigh surface-wave speed.

INTRODUCTION

The economic importance of fracture is sufficient to explain the widespread interest in this classical field among engineers. The integrity of aircraft and pressurized nuclear reactors, together with the interest in subterranean fracture for hydrocarbon recovery, are problems of current interest. At the same time fracture has not yet attracted much interest from physicists¹ who could contribute a sound microscopic understanding of the mechanisms underlying the macroscopic phenomena of fracture. Several microscopic "models" of fracture have been described² but these models typically incorporate the artificial features of noncentral forces and preassigned fracture loci or very complicated force laws.³ Before introducing these inessential complexities, we prefer to understand the consequences of simple central forces in a classical crystal undergoing fracture.

Because we wish to incorporate fracture into the broadening range of subjects clarified by statistical mechanics and molecular dynamics, we study the simplest possible atomic model which can illustrate the fracture phenomena, mass points interacting with linear-force Hooke's-law springs in a two-dimensional triangular lattice. The thermodynamic and lattice-dynamic properties for this crystal are already well known.⁴ This model bears a close resemblance to the simplest "finite-element" model used by structural engineers in macroscopic stress analysis. The equivalence is demonstrated in Appendix A.

Recent progress in simulating mass, momentum, and energy transfer with nonequilibrium molecular dynamics⁵ makes us optimistic that fracture, another nonequilibrium problem, can be treated

successfully too. Here we summarize results of equilibrium and nonequilibrium fracture studies which demonstrate the wealth of new information readily available with today's fast computers.

MODEL

All of our crystals have the triangular (sixfold coordination) structure shown in Fig. 1. The particles in these crystals interact with a truncated parabola, or with a double-parabola potential,² or with a parabola-linear potential, as shown in Fig. 2. The microscopic variables characterizing such a system are the particle mass m , the interparticle spacing d , the spring constant k , and the well width w .

If we write the macroscopic stress tensor for such a crystal in terms of the Lamé constants λ and η

$$\underline{\sigma} = \lambda \vec{\nabla} \cdot \vec{u} \underline{I} + \eta (\vec{\nabla} \vec{u} + \vec{\nabla} \vec{u}^T), \quad (1)$$

then the two constants are equal: $\lambda = \eta = \sqrt{3} k/4$. (Detailed calculation shows that the two shear moduli for the triangular lattice are equal. Thus, for elastic properties, the *isotropic* form of the stress tensor can be used. The equivalence is demonstrated in the paper by Hoover, Ashurst, and Olness.⁴) The two-dimensional calculations correspond to three-dimensional plane-strain calculations with the same Lamé constants or to three-dimensional plane-stress calculations with $\lambda' = 2\eta$ replacing λ .

Several kinds of boundary conditions can be imposed on the crystal. The simplest of these, constant-stress, periodic, and constant-displacement boundaries, will be discussed here. Boundaries which correspond to linearly increasing stress and strain are also of interest in fracture problems.⁶

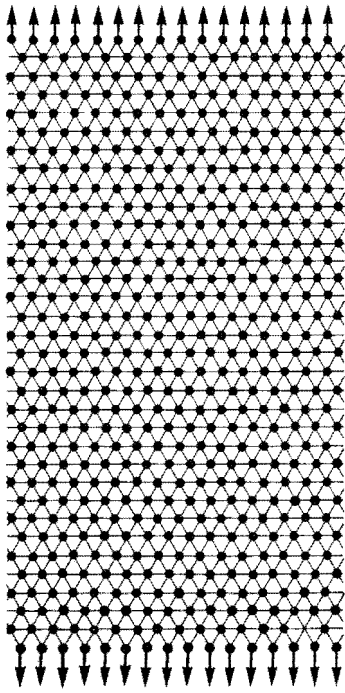


FIG. 1. A 512-particle close-packed triangular lattice of mass points joined by Hooke's-law springs. The particles interact with 32 additional boundary particles which in turn interact with a constant external force, $+\sigma d$ on the upper-boundary particles and $-\sigma d$ on the lower-boundary particles. The effects of cracks on energy, entropy, and structure are studied by breaking some of the bonds linking neighboring particles. Periodic boundaries link the left and the right sides of the crystallite, maintaining an average horizontal spacing equal to that found in a stress-free crystal.

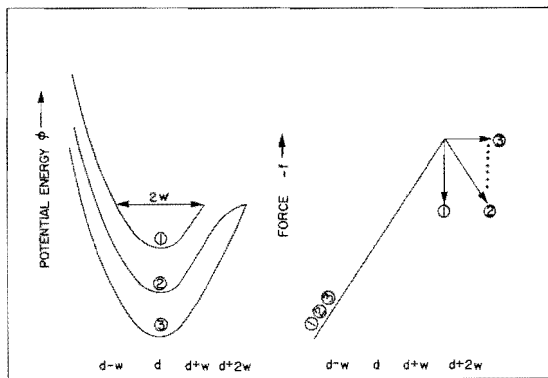


FIG. 2. Interparticle potentials $\phi(r)$ and forces $f(r) = -\phi'(r)$. All of these potentials have the same curvature at the minimum, $k = \phi''(r_{\min} = d)$, and hence the same linear elastic properties. The tensile strength of crystals composed of particles interacting with these potentials depends on the potential width w . The single-parabola potential (1) corresponds to linear elasticity theory in the limit that d and w/d both approach zero.

STATIC RESULTS

We began by studying the static properties of crystals with several contiguous broken bonds. The horizontal boundaries were maintained at a constant stress and the vertical boundaries were joined periodically as shown in Fig. 1. For such cracks, in an elastic continuum, the stress field and stored elastic energy are well known.⁷

In Table I and Figs. 3 and 4 we show the variation of stored energy and crack structure with crack length L in 512-particle crystals. These results are consistent with elasticity-theory predictions: The energy varies as the square of the crack length, and the crack shape resembles an ellipse.⁷

In these static calculations the interparticle forces were taken as linear functions of the particle displacements up to a maximum stretch $w \ll d$ at which the force discontinuously drops to zero (as in the type-1 potential shown in Fig. 2).

Macroscopic elasticity theory predicts that the stress and strain fields in the vicinity of the crack tip vary as $r^{-1/2}$, where r is the distance from the tip, diverging at the tip itself.⁸ The coefficient of the $r^{-1/2}$ divergence is proportional to the "stress-intensity factor," the value of which, at failure, is tabulated as a material property K_{Ic} . From macroscopic elasticity theory⁸ K_{Ic} is $(\pi/2)^{1/2} \sigma_f L^{1/2} = 1.253 \sigma_f L^{1/2}$, where σ_f is the perpendicular tensile stress at failure for a large plate containing a crack of length L far from the plate boundary. Analysis of our results (based on extrapolating the stretch in the spring next to the crack to the large-

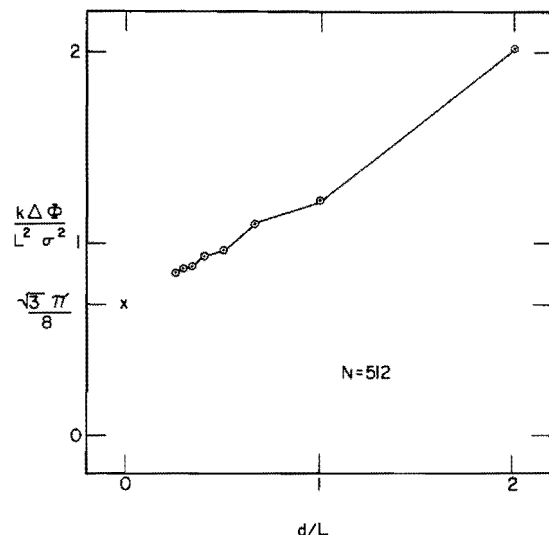


FIG. 3. Energy increase, relative to an uncracked crystal, for stressed 512-particle crystals with $2L/d$ broken bonds. The prediction of macroscopic fracture mechanics, for a crack small relative to crystal dimensions, is the intercept, marked with an x .

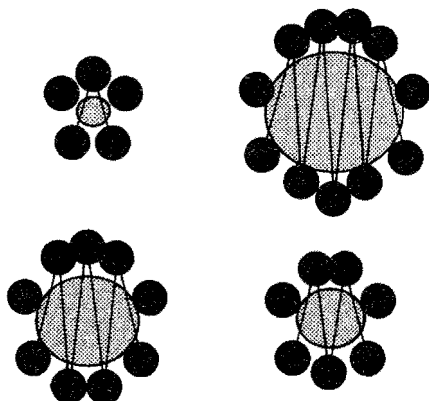


FIG. 4. Displacements in the neighborhood of cracks with 2, 4, 6, and 8 broken bonds. The particles have been drawn as filled circles, which touch one another in the stress-free crystal. The displacements in the stressed crystal slightly exceed the predictions of macroscopic linear elasticity theory. The predicted shape for a small crack in a large crystal is elliptical, with a major-to-minor-axis ratio of $(k/\sigma)/\sqrt{3}$. The more complicated expression for a crack length equal to one-fourth the system width predicts a crack opening about 3% wider than the large-crystal ellipse. The crack openings predicted by linear elasticity theory are shown as shaded areas in the figure. It should be emphasized that the scale of the displacements is arbitrary (but infinitesimal) in linear elasticity, and has thus been greatly exaggerated here for clarity.

L limit) identifies the failure stress σ_f for our structure as $0.89(d/L)^{1/2}$ times the ideal crack-free failure stress of $\sqrt{3} k(w/d)$. If, for example, the springs break at a 10% extension ($w/d=0.1$), σ_f is $0.154k(d/L)^{1/2}$ and the critical stress-intensity factor is $0.19kd^{1/2}$.

Bonds using a 6-12 Lennard-Jones interaction "break" at a 10.9% extension, in the sense that the force required to stretch the bond beyond that extension is a decreasing function of r . Because our static calculations use linear forces, with the assumption $w \ll d$, our use of those results to estimate critical stress-intensity factors for finite w is only approximate. Nevertheless, detailed calculation shows that the calculated stress-intensity

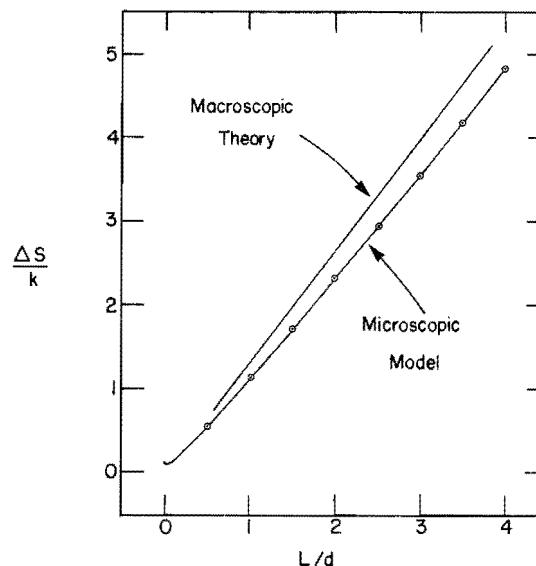


FIG. 5. Entropy increase, relative to an uncracked crystal, for crystals with $2L/d$ broken bonds. These broken bonds correspond to a horizontal crack of length L lying between the 17th and 18th rows of particles shown in Fig. 1. For large L most of the entropy increase corresponds to the surface entropy for a surface of length $2L$ (indicated by the straight line "macroscopic theory" in the figure).

factor, using the linear forces, lies within 2% of that calculated exactly for $w=0.1d$.

Because the fracture process is irreversible, the stress must drop below $0.89(d/L)^{1/2}\sigma_f$ in order for the crack to shrink. Analysis of our static results shows that open cracks heal again at a stress $0.24(d/L)^{1/2}$ times the theoretical strength. Thus there is a wide range of stresses within which a crack of length L neither grows nor shrinks. This phenomenon is called "lattice-trapping" by Thomson and co-workers.²

Some new features are present in our calculations. We have calculated the entropy contribution of a crack to the crystal by comparing the traces of the dynamical matrix before and after the crack is introduced.⁴ The entropy calculation could in principle be carried out for an elastic continuum,

TABLE I. Energy and entropy changes induced in a 32-row, 512-particle crystal (see Fig. 1) by introducing a crack of length L . The increase in energy corresponds to constant stress σ applied at the upper and lower boundaries of the crystal. The energy data are of the form $k\Delta\phi/\sigma^2d^2 = 0.68 + 0.6d/L$. The entropy data lie within 0.01 of the expression $\Delta S/k$ (Boltzmann) $= 1.354(L/d) - 0.363(L/d)^{1/2} + 0.127$. The large- L limiting energy agrees with the known result from elasticity theory⁷ and the large- L entropy agrees with the surface-entropy calculations of Ref. 4. The entropy calculations here are based on the method used in that reference.

Crack length/ d	$\frac{1}{2}$	1	$1\frac{1}{2}$	2	$2\frac{1}{2}$	3	$3\frac{1}{2}$	4
$k\Delta\phi/\sigma^2d^2$	0.5024	1.2127	2.4871	3.8585	5.8711	7.9476	10.7332	13.5652
$\Delta S/k$ (Boltzmann)	0.5488	1.1124	1.7157	2.3195	2.9391	3.5588	4.1866	4.8145

though only with difficulty. In Fig. 5 we show the results, obtained as is indicated in Table I. The entropy contains not only the expected linear dependence on crack length, identical to the surface entropy previously calculated for the triangular lattice,⁴ but also a term of order $L^{1/2}$, the contribution of the crack tips. The fact that energy varies as L^2 and entropy as L suggests that the usual practice in fracture mechanics, ignoring entropy, can be justified in macroscopic calculations where L is large.

The static results also show that the next bond to break has nearly the same stretch as do three other bonds in the crystal. Figure 6 indicates that in many cases the static-lattice calculations suggest that cracks will propagate by leapfrog propagation, in which springs once-removed from the crack tip break before the adjacent springs. These static considerations also suggest, in accord with experiment, that as fracture propagates through a crystal a relatively wide-spread damaged region can result, with a surface energy exceeding that of a clean cleavage crack.

DYNAMIC RESULTS

We study dynamic properties of fracturing crystals by using Verlet's solution of the equations of motion,⁵ replacing the particle accelerations by centered second-difference approximations:

$$\frac{d^2 \bar{r}_i(t)}{dt^2} = [\bar{r}_i(t+dt) - 2\bar{r}_i(t) + \bar{r}_i(t-dt)]/(dt)^2. \quad (2)$$

A choice of $dt = 0.1(m/k)^{1/2}$ typically conserves energy with four-figure accuracy. Some calculations were carried out with smaller time steps to con-

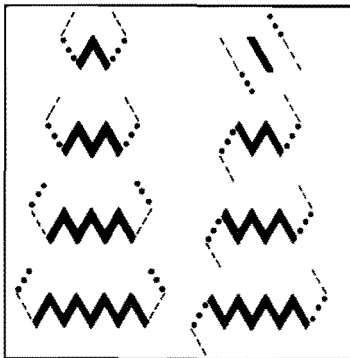


FIG. 6. Predicted quasistatic fracture direction for a stressed 512-particle crystal. The initially broken bonds (1, 2, . . . , 8) are indicated by heavy lines. The most-highly-strained bonds are indicated by dashed lines—by symmetry there are two such bonds in each case. The next-most-highly-strained bonds are indicated by dots. Only in the cases that 6 or 8 bonds are initially broken does the crack “propagate” directly from its tip. Dynamic and nonlinear effects both inhibit the leapfrog propagation.

firm that the results are insensitive to this choice.

We began by exploring the propagation of cracks in crystals with the constant-stress boundaries shown in Fig. 1. The boundaries soon became grossly deformed (as shown in Fig. 7). This deformation could be controlled by boundary damping,⁹ but the growing stress concentration (increasing as the square root of the crack length⁶) produced nonsteady hard-to-interpret results. Accordingly we adopted instead horizontal-strip boundary conditions with fixed vertical and horizontal boundaries. The horizontal boundaries impose a tensile stress on the crystal. The vertical boundaries are fixed with the horizontal spacing corresponding to a stress-free crystal. These conditions, together with related variants in which the vertical stress increases or decreases linearly along the strip, have been considered previously.⁹ They make it possible to observe steady-state fracture and, for this reason, are of fundamental importance.

Using the constant-displacement fixed boundaries we were able to achieve steady propagation, although only with some care. The calculations were carried out in three steps: initialization, relaxation, and propagation. First, several contiguous bonds were “broken” near the crystal's left boundary. These broken bonds are ignored in calculating the accelerations used in Eq. (2). Second, the crystal was partially relaxed, building up stress concentration at the crack tip, by following the time development for a time $10(m/k)^{1/2}$. During this relaxation phase a critically damped dashpot was introduced in parallel with each of the unbroken Hookean springs. At the end of the relaxation phase the breaking strength of the springs was set, by choosing w such that the spring adjacent to the incipient crack would break. Then the dashpots were removed and the crack was allowed to propagate. It was verified that the velocities found for finite strips n -rows high and $5n$ -particles long provide velocities which are not significantly different from the long-strip case. The results are also in-

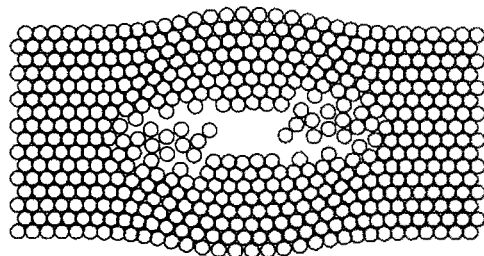


FIG. 7. Typical appearance, at long times, for a crystal undergoing fracture with constant-stress boundaries in the absence of boundary damping. The bulging of the boundaries can be inhibited by viscous damping.

sensitive to the number of bonds initially broken. This was typically chosen to equal twice the number of rows n so that the initial crack was of length $\frac{1}{2}nd$.

Figure 8 shows a typical fracture pattern found with purely linear springs, in which w is treated as infinitesimal relative to d in solving the equations of motion. The nearly isolated row of particles is typical of the purely linear system and is due to the fact that the springs do not sense rotation of the interatomic force directions. The tip of the crack in these perfectly linear crystals also has a relatively artificial appearance.

In order to test the dependence of propagation velocity on w we considered a range of widths from nearly zero to about four-tenths of d . In order that a regular close-packed lattice be the least-energy state of the system, the repulsive forces need to be sufficiently strong. Otherwise the crystal could in principle exhibit thermodynamic instability and collapse. For the single-parabola Hooke's-law potential to avoid this hazard of collapse, w can be no greater than $d/13^{1/2} = 0.277d$ in two dimensions and $d/25^{1/2} = 0.200d$ in three dimensions. (The limits are $0.196d$ and $0.141d$ for the double-parabola potential.) Results, for cracks just able to propagate, are plotted in Fig. 9 for both the single-parabola and double-parabola potentials. See Table II. These show that, as might be expected, the additional binding energy of the double-parabola well retards the crack, although by somewhat less than the $\sqrt{2}$ factor a simple energy-balance theory such as Griffith's might suggest.⁷ Our results show that only 38% of the initial strain energy in the crystal ends up as surface energy in the single-parabola case. Because Griffith's theory is based on the equivalence of the strain energy and the surface energy it can be expected to provide only semiquantitative estimates.

An extrapolation of the single-parabola results to zero width (corresponding to linear elasticity theory) indicates a limiting fracture velocity of about $0.3d(k/m)^{1/2}$. There are two approaches

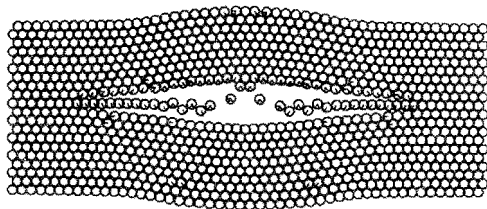


FIG. 8. Typical appearance of a crystal in which the forces are calculated as linear functions of particle displacements (ignoring the effects of bond rotation). Non-linear terms, of order w/d , inhibit the appearance of isolated rows of particles.

which provide estimates close to this value. One is Mott's,¹ based on analyzing the kinetic-energy field in the vicinity of a propagating crack, resulting in the estimate $0.40d(k/m)^{1/2}$. A second estimate might be based on the idea that cracks should travel at the Rayleigh (surface-wave) velocity because a crack corresponds to newly created surface. In this event one might expect that dispersion of the surface waves would be instrumental in limiting the crack velocity to that of the shortest-wavelength Rayleigh wave. In Appendix B we calculate the dispersion relation for Rayleigh waves in the triangular crystal, using a method based on earlier work for the simple-cubic crystal,¹⁰ and find a sinusoidal dispersion relation with the slowest wave phase velocity equal to $0.36d(k/m)^{1/2}$.

The increase in speed from the elastic-theory result as w increases, shown in Fig. 9, should not be surprising. Two separate effects should lead to increased speeds as the well width increases. Both can be traced to the loss of crystal symmetry (finite-strain effects). First, the vibrational frequency in the 60° direction of the diagonal bonds increases. Second, larger widths imply that after a bond has broken the recoil will have a greater projection along the line of the next bond to break. Both effects lead to velocity increases of order w/d .

The static-lattice analysis just outlined could only be strictly valid in a highly strained crystal where crack propagation can outrun lattice relaxation.² We have investigated this supersonic-

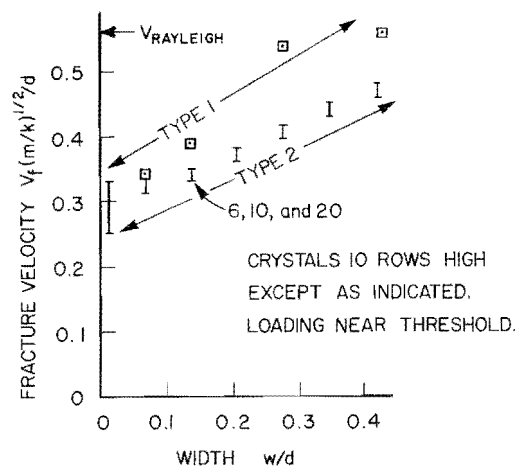


FIG. 9. Steady fracture velocity for a series of potentials of types 1 and 2 (see Fig. 2). All the data correspond to crystals just beyond the threshold loading for fracture. Except as indicated the data refer to 500-particle strips with initial crack lengths of $10d$. The statistical uncertainty of the data is indicated by the size of the plotting symbols. Portions of the fracture history at the beginning and end of the fracture have been omitted in determining those speeds.

propagation regime [with v_f greater than the longitudinal sound speed, $1.061d(k/m)^{1/2}$], and find that the theoretical result,

$$v_f(\text{supersonic}) = \frac{1}{4}d(k/m)^{1/2}(w/\delta)^{1/2}, \quad (3)$$

describes the data quantitatively (Fig. 10). In (3)

TABLE II. Propagation velocities v_f of cracks in systems NR -rows high and NL -particle-diameters long. The initial state of the system is achieved by starting with a perfect stress-free crystal, fixing the x coordinates of left-hand and right-hand boundary particles, applying the strain $\epsilon_{yy} = \epsilon$, fixing the y coordinates of the top and bottom rows of particles, "breaking" b bonds, [that is, ignoring the forces from these bonds in solving Eq. (2)], and allowing the system to relax with viscous critically damped dashpots in parallel with the unbroken bonds for a time $10(m/k)^{1/2}$. Then the dynamical evolution of the system is followed with the dashpots removed. The potential type (see Fig. 2) and well width are also listed. For all of these crystals the longitudinal sound speed is $(\frac{3}{8})^{1/2}(k/m)^{1/2}d$, the transverse sound speed is $(\frac{3}{8})^{1/2}(k/m)^{1/2}d$, and the Rayleigh-wave speed is $(3 - \sqrt{3})^{1/2}(k/m)^{1/2}d$. Uncertainties in v_f are generally $\pm 0.01(k/m)^{1/2}d$. The time step used was generally $0.1(m/k)^{1/2}$.

NR	NL	b	ϵ	Type	w/d	$v_f(m/k)^{1/2}/d$
10	50	19	0.05	1 ^a	0.068	0.34
10	50	19	0.10	1	0.137	0.39
10	50	19	0.20	1	0.277	0.54
10	50	19	0.30	1	0.427	0.56 ^b
10	50	19	0.01	2	0.0125	0.29 ± 0.04 ^c
10	50	19	0.05	2	0.066	0.337 ^d
10	50	19	0.05	2	0.068	0.315
6	50	11	0.129	2	0.137	0.34
10	50	19	0.10	2	0.137	0.345
10	50	19	0.10	2	0.137	0.347 ^e
20	50	40	0.0707	2	0.137	0.34
10	50	19	0.10	2	0.133	0.32 ± 0.03 ^f
10	50	19	0.15	2	0.207	0.372
10	50	19	0.20	2	0.277	0.407
10	50	19	0.25	2	0.348	0.440
10	50	19	0.30	2	0.419	0.470 ^g

^a Fractures in type-1 crystals broke off-center after about 12 bonds had broken.

^b The shape of the crack tip resembles a large keyhole in this case, so that finite-width boundary effects are probably large.

^c Propagation for this very-narrow-well crystal was somewhat erratic. An otherwise identical calculation using the type-2 potential produced an erratic crack with velocity about $0.3(k/m)^{1/2}d$.

^d This crack broke off-center after about six bonds had broken.

^e For this calculation a time step of $0.05(m/k)^{1/2}$ was used.

^f This crack bifurcated and came to a halt.

^g No second-neighbor interactions are included for any of the large- w calculations.

δ is the distance necessary for a bond to stretch before breaking—the initial stretch is $w - \delta$. See Table III.

We have studied three different modes of crack arrest. The first of these demonstrates that the double-parabola potential is less prone to fracture than the single parabola (although they have identical elastic properties). Two crystals, 10-rows high and 50-diameters long, were loaded so that the diagonal bonds, far from the 19 initially broken, were stretched to $0.597w$. In the single-parabola case, the fracture propagated the additional distance $40d$ across the entire crystal with a velocity of $0.435d(k/m)^{1/2}$. In the double-parabola case, the fracture propagated only a distance $8d$, with a velocity of $0.357d(k/m)^{1/2}$, then bifurcated (starting two cracks), and stopped. The final configuration is shown in Fig. 11. A similar comparison was carried out between the double-parabola and the parabola-linear potentials (potentials 2 and 3 of Fig. 2). With $w = 0.1d$ and an initial strain of 0.088 the double-parabola crystal fractured completely across, with velocity $0.34d(k/m)^{1/2}$, while the parabola-linear potential failed to propagate. Increase of the initial strain to 0.11 resulted in a higher velocity for the double parabola, $0.523d \times (k/m)^{1/2}$, and to a propagation length of $14.5d$ for the parabola-linear potential, at which point that crack stopped. An even greater strain, 0.125, was required to see propagation for the deeper potential; an unsteady velocity $\sim 0.38d(k/m)^{1/2}$ was recorded. This same loading greatly overdrives the double-parabola potential, resulting in a fracture velocity $0.82d(k/m)^{1/2}$ exceeding the transverse sound velocity $0.612d(k/m)^{1/2}$. Figure 12 shows two stages in the fracture of a crystal containing a vacancy. The vacancy relieves the

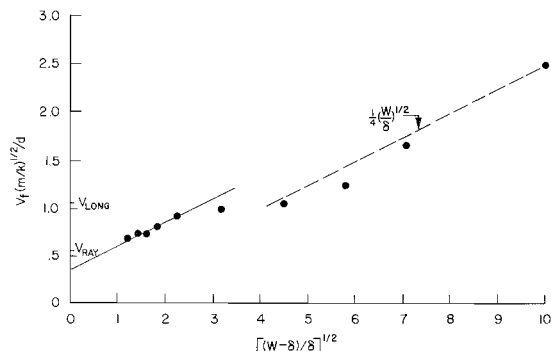


FIG. 10. Fracture velocity, using linear forces, for a series of 500-particle crystals. At very high initial loadings (δ approaches zero, where δ is the stretch at failure less the initial stretch in a diagonal bond) the results reproduce Eq. (3) of the text. Even at the greatest δ shown the propagation velocity exceeds the long-wavelength Rayleigh velocity $0.56d(k/m)^{1/2}$.

TABLE III. Propagation velocities v_f of cracks in 500-particle crystals with linear forces. The well width w is treated as infinitesimal relative to d in these calculations. The crystals were initially relaxed, with critically damped dashpots parallel to the unbroken springs and with a fixed crack length of $10d$. Following a relaxation time of $10(m/k)^{1/2}$ the dashpots were removed and the crack was allowed to propagate. The velocities found are expressed in terms of the well width w and the additional stretch δ required to break the springs. Results for small δ/w obey relation (3) of the text. The subsonic cracks, with smaller δ/w ratios, extrapolate roughly to a zero-strain velocity of $0.36(k/m)^{1/2}d$. This intercept may be misleading because the morphology of the cracks changes for δ values larger than those in the Table.

$\delta/(w - \delta)$	0.675	0.500	0.400	0.300	0.200	0.100	0.05	0.03	0.02	0.01
$v_f(m/k)^{1/2}/d$	0.67 ^a	0.733	0.738	0.806	0.926	1.00 ^b	1.06	1.25	1.67 ^c	2.50 ^d

^a This velocity was also reproduced, within about 1% at the same prestrain, in crystals 14- and 20-rows high.

^b In the linear calculations particles can remain connected with their neighbors despite a large displacement perpendicular to their original bond direction. Thus for the subsonic linear-force "fractures," unrealistic damage, such as that shown in Fig. 8, results.

^c At this relatively high prestrain a nonlinear calculation, with $w=0.137d$, gave the same fracture velocity.

^d At or above this prestrain the measured velocities agree with the asymptotic relation (3) of the text.

elastic strain in its neighborhood, first attracting, and finally stopping the advancing crack.

CONCLUSION

Our results show that even the simplest crystal models, with Hooke's-law forces, are sufficiently complicated to provide a host of interesting physical phenomena, including varying propagation velocities, widespread damage, while remaining susceptible to exact analysis. We expect that further study of these systems will eventually provide as complete an understanding of fracture mechanics as now exists for the equilibrium and linear transport properties of simple systems.

ACKNOWLEDGMENT

We are grateful to Nancy Barnes, Bill Delameter, Doug Norris, Clarence Parkison, Marvin

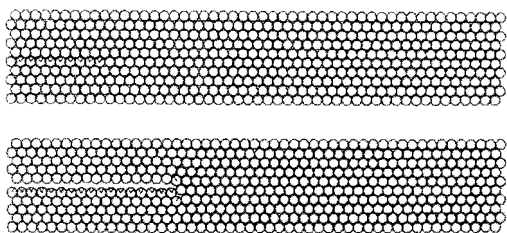


FIG. 11. Illustration of the effect of the smoother double-parabola potential (2 in Fig. 2) in inhibiting fracture. The crack shown, initially of length $10d$, grew to a length of $18d$, bifurcated, and stopped. The lines drawn within the particle circles indicate broken bonds. A single-parabola potential (1 in Fig. 2) behaves differently under identical loading conditions, propagating fracture across the entire crystal at a velocity $0.435 d(k/m)^{1/2}$.

Ross, and Dave Young for useful advice, literature references, and technical assistance. Most of the calculations were carried out on the Sandia Livermore CDC 6600 computer. Some of the static calculations were carried out on the now defunct Department of Applied Science CDC 3400 computer.

APPENDIX A: RELATION TO THE FINITE-ELEMENT METHOD

The finite-element method is often used by structural engineers in computer analyses of the thermal and mechanical behavior of complicated structures. The structure in question is divided up into zones ("elements") within which displacements, velocities, temperatures, etc., are assumed to vary in a simple way. The transient, or steady-state, problem is then solved by matrix diagonalization. Systems with thousands of discrete elements can be treated.

Consider now a simple finite-element descrip-

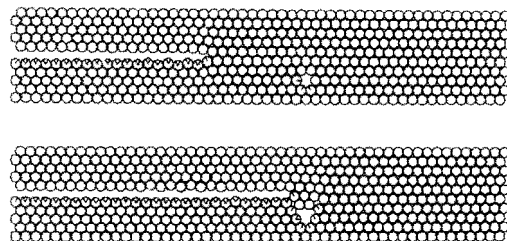


FIG. 12. Illustration of the effect of a vacancy in inhibiting fracture. Initially the 499-particle crystal contained one void and a relaxed crack of length $10d$. The crack was allowed to run, and did so until stopped by interaction with the vacancy.

tion of our elastic model crystal. If we use the springs joining our Hookean masses as element boundaries and if we assume that the displacement *within* each of the equilateral triangular elements is a linear function of \vec{r} , then the six constants in the relation

$$\vec{u} = \vec{c} + \underline{C} \cdot \vec{r}$$

can all be expressed in terms of the three sets of xy coordinates forming the vertices of the element. These displacements can then be introduced into the equations of macroscopic linear elasticity to calculate the strain energy of the triangular element in question.

In order to compare the elastic energy according to this linear finite-element theory with the energy from the Hooke's-law springs, we first express the Lamé constants λ and η in terms of the spring constant k :

$$\lambda = \eta = \frac{1}{4}\sqrt{3}k.$$

The energy for any triangular finite element is then the product of the elastic energy density and the element volume $\sqrt{3}d^2/4$,

$$\phi = \frac{3}{16}kd^2 \left[\frac{1}{2}(\vec{\nabla} \cdot \vec{u})^2 + \frac{1}{4}(\vec{\nabla} \vec{u} + \vec{\nabla} \vec{u}^T) : (\vec{\nabla} \vec{u} + \vec{\nabla} \vec{u}^T) \right].$$

If we instead take the microscopic view of lattice dynamics we associate half of the potential energy of the three springs bounding a finite element with the energy of that element

$$\phi = \sum_{\frac{1}{2}}^3 \frac{1}{4}k\delta'^2,$$

where δ' is the change in spring length from the least-energy state.

It is a straightforward and tedious, but rewarding, task to show that these two dissimilar expressions for the energy ϕ are *identical*.¹¹ Thus the least-energy configuration for a discrete crystal described either from the lattice viewpoint or

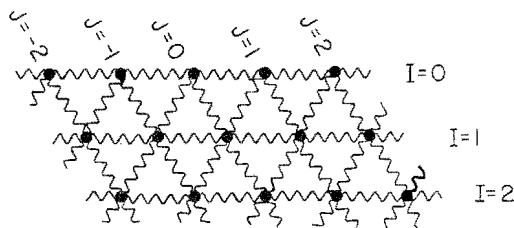


FIG. 13. Crystal geometry used to derive the Rayleigh-wave dispersion relation of Appendix B. The top row of particles is a free surface. Rayleigh waves can travel along the surface (for wavelengths greater than $8.38d$). Shorter-wavelength solutions are also found (generalized Rayleigh waves). All of the solutions obey the dispersion relation $m\omega^2 = k(3 - \sqrt{3})\sin^2\theta$, where the wavelength is $\pi d/\theta$.

from the isotropic continuum viewpoint (using linear equilateral finite elements with sidelength equal to the interatomic spacing d) is the same. Evidently this energy correspondence between a simple crystal lattice with nearest-neighbor Hookean springs and an isotropic elastic continuum is restricted to two dimensions; neither of the simple close-packed three-dimensional lattices (face-centered cubic and hexagonal close-packed) is isotropic.

The equivalence is interesting, not only for pedagogical reasons, but also because it might suggest useful approximations for generalizing finite-element energies in the case of imperfect lattices.

APPENDIX B: RAYLEIGH-WAVE DISPERSION RELATION

Begin by labeling the particles in a periodic crystal with indices I and J , as shown in Fig. 13. We will ultimately discard those particles with negative values of I so that then the row $I=0$ will correspond to the crystal surface. If we assume a motion of the form

$$(u, v)_{I,J} = (U, iV) \exp[-qI + i\theta(I + 2J) + i\omega t],$$

then solutions with real U , V , q , and θ correspond to periodic waves, with wavelength $\pi d/\theta$ in the x direction, decaying exponentially in the y direction. In the long-wavelength limit we expect to find the continuum solutions¹⁰

$$\begin{aligned} \omega &= 1.12603(k/m)^{1/2}\theta \quad \text{for } q_1 = 1.46789\theta, \\ q_2 &= 0.68125\theta. \end{aligned}$$

The calculation proceeds in two steps. First the dispersion relation linking ω , q , and θ ,

$$\begin{aligned} m\omega^2/k &= 3 - 2cC - c' \pm [(c' - cC)^2 - 3s^2S^2]^{1/2}; \\ c &= \cos\theta; \quad s = \sin\theta; \quad c' = \cos 2\theta; \\ C &= \cosh q; \quad S = \sinh q, \end{aligned}$$

is solved for q . These solutions can then be checked to see whether or not the x and y forces on particles in row 0 due to those in row -1 vanish. If these forces *do* vanish, then row -1 can be ignored and we have a surface-wave solution. The condition for the vanishing surface forces is

$$\frac{R_1(ce^{q_1} - 1) - \sqrt{3}se^{q_1}}{R_2(ce^{q_2} - 1) - \sqrt{3}se^{q_2}} = \frac{R_1se^{q_1} + \sqrt{3}(ce^{q_1} - 1)}{R_2se^{q_2} + \sqrt{3}(ce^{q_2} - 1)},$$

where R_i is the ratio of U to V in the solution corresponding to q_i . An expansion in powers of q and θ shows that the long-wave limit values of R_1 and R_2 are -1.17996 and -0.39332 , reproducing the continuum solution. For larger q we had a computer find the solution. For values of the wave num-

ber θ less than $\cos^{-1}(\frac{3}{4})^{1/4} = 21.47^\circ$ (corresponding to wavelengths greater than 8.38 particle diameters), Rayleigh-wave solutions were found with two distinct real positive q_i . Particle displacements fall off exponentially with penetration into the crystal in this case. These solutions for q change in form, becoming complex conjugates, at $\theta = 21.47^\circ$ with the particle displacements falling off as a damped periodic disturbance for shorter

wavelengths. A remarkable feature of the computer-generated solution for ω as a function of θ is its simple form:

$$m\omega^2/k = (3 - \sqrt{3})\sin^2\theta.$$

Thus the dispersion relation has the same form as the bulk-wave dispersion relation for a one-dimensional chain.

*This work was supported by the United States Atomic Energy Commission and by its successor, the Energy Research and Development Administration. A summer visitor to the Lawrence Livermore Laboratory, Professor Robert C. Cook of Lafayette College, Easton, Pennsylvania, participated in the static work. A preliminary account of some of these results was presented at the Fifth Atlas Computer Symposium "Computational Physics of Liquids and Solids" at the Queen's College, Oxford, 12-14 April 1975.

¹See, however, N. F. Mott, *Engineering (Lond.)* 165, 16 (1948); D. K. Roberts and A. A. Wells, *ibid.* 178, 820 (1954).

²J. E. Sinclair and B. R. Lawn, *Proc. R. Soc. Lond. A* 329, 83 (1972); R. Thomson, C. Hsieh, and V. Rana, *J. Appl. Phys.* 42, 3154 (1971); C. Hsieh and R. Thomson, *ibid.* 44, 2051 (1973); E. Smith, *ibid.* 45, 2039 (1974); W. T. Sanders, *Eng. Fracture Mech.* 4, 145 (1972); J. H. Weiner and M. Pear, *J. Appl. Phys.* 46, 2398 (1975).

³M. F. Kanninen and P. C. Gehlen, in *Interatomic Potentials and Simulation of Lattice Defects*, edited by P. C. Gehlen, J. R. Beeler, and R. I. Jaffee, (Plenum, New York, 1972).

⁴A. Beyerlein and Z. W. Salsburg, *J. Chem. Phys.* 47, 3763 (1967); D. A. Huckaby, *ibid.* 54, 2910 (1971); W. G. Hoover, *ibid.* 49, 1981 (1968); W. G. Hoover,

A. C. Hindmarsh, and B. L. Holian, *ibid.* 57, 1980

(1972); P. Dean, *Proc. Camb. Philos. Soc.* 59, 383 (1963); W. G. Hoover, W. T. Ashurst, and R. J. Olness, *J. Chem. Phys.* 60, 4043 (1974).

⁵W. T. Ashurst and W. G. Hoover, *Phys. Rev. A* 11, 658 (1975). See also, W. G. Hoover and W. T. Ashurst, *Theoretical Chemistry, Advances and Perspectives 1* (Academic, New York, 1975).

⁶T. L. Paxson and R. A. Lucas, in *Dynamic Crack Propagation*, edited by George C. Sih (Noordhoff, Leyden, 1973), p. 415.

⁷A. J. M. Spencer, *Int. J. Eng. Sci.* 3, 441 (1965); P. Tong and T. H. H. Pian, *Int. J. Solids Struct.* 9, 313 (1973); A. A. Griffith, *Phil. Trans. R. Soc. Lond. A* 221, 163 (1920); W. T. Koiter, *Ing.-Arch.* 28, 168 (1959).

⁸H. Tada, P. C. Paris, and G. R. Irwin, *The Stress Analysis of Cracks Handbook* (Del Research Corporation, Hellertown, Pennsylvania, 1973).

⁹J. B. Gibson, A. N. Goland, M. Milgram, and G. H. Vineyard, *Phys. Rev.* 120, 1229 (1960).

¹⁰Lord Rayleigh, *Proc. Lond. Math. Soc.* 17, 4 (1887); Y. C. Fung, *Foundations of Solid Mechanics*, p. 178 (Prentice-Hall, Englewood Cliffs, N. J., 1965); D. C. Gazis, R. Herman, and R. F. Wallis, *Phys. Rev.* 119, 533 (1960).

¹¹A. Irennikoff, *J. Appl. Mech.* 8, A-169 (1941).